

UNIVERSITY OF WATERLOO  
Faculty of Science

*Nonlocal Translationally Invariant  
Nuclear Density*

Theory Group - TRIUMF  
Vancouver, British Columbia

prepared by

Michael Gennari  
#20552297  
3B Mathematical Physics  
April 2017

295 Lester Street  
Waterloo, ON  
N2L 3W6

May 7, 2017

Brian McNamara  
Physics and Astronomy  
University of Waterloo  
Waterloo, Ontario  
V6T 2A3

Dear Brian McNamara,

I have prepared the enclosed report Nonlocal Translationally Invariant Nuclear Density as my 3B Work Report for TRIUMF. This report, the second of four work reports that Co-operative Education Program requires that I complete as part of my Co-op BSc degree requirements, has not received previous academic credit.

As a Researcher in Theoretical Nuclear Physics at TRIUMF, I assisted Dr. Petr Navrátil in generalizing his work on local nuclear densities to a nonlocal form, and implementing code for improving the physical accuracy of nuclear densities. Additionally, I derived an implementable version of the kinetic density of a nucleus, allowing our group to further benchmark the more physically accurate nuclear density the implications it may have on theoretical nuclear physics.

The Theory Group at TRIUMF, led by my supervisor Petr Navrátil, focuses on *ab initio* approaches to theories in nuclear and particle physics.

This report was written entirely by myself and has not received previous academic credit at any institution. I would like to thank Dr. Petr Navrátil and Dr. Angelo Calci for assisting me with my work throughout the term and for providing valuable guidance in this research project. I give permission to TRIUMF to keep this report on file and use it for internal reporting and external reporting including publication. I would like to thank you for your assistance in preparing this document.

Sincerely,



Michael Gennari

Encl.

# Nonlocal Translationally Invariant Nuclear Density

## Abstract

Nonlocal nuclear density is derived from the shell model one-body densities by generalizing the local density operator to a nonlocal form with separate coordinates acting on the initial and final states of the wavefunction. The translational invariance is constructed by removing the spurious center of mass (COM) component of the harmonic oscillator wavefunction, which is an unphysical contribution to the density. This provides a more physically accurate density allowing the *ab initio* no-core shell model (NCSM) nuclear structure to be used analytically in high energy nuclear reactions and density functional theory. The groundstate local and nonlocal density of  $^4\text{He}$ ,  $^6\text{He}$ , and  $^{16}\text{O}$  are calculated to display the effects of COM removal on predicted nuclear structure. It is expected that amplified effects of the COM removal can be seen in related quantities like kinetic density, which is dependent on gradients of the nonlocal nuclear density.

# Table of Contents

<b>1.0 Introduction . . . . .</b>	<b>1</b>
<b>2.0 Analysis . . . . .</b>	<b>2</b>
2.1 Nonlocal Translationally Invariant Nuclear Density . . . . .	2
2.1.1 Background . . . . .	2
2.1.2 Application to $^4\text{He}$ , $^6\text{He}$ , and $^{16}\text{O}$ . . . . .	5
2.1.3 $N_{\max}$ Convergence . . . . .	9
2.2 Derivative of Radial Harmonic Oscillator . . . . .	10
2.3 Kinetic Density . . . . .	11
2.3.1 Derivation . . . . .	12
2.3.2 Kinetic Density of $^{16}\text{O}$ . . . . .	15
<b>3.0 Conclusions . . . . .</b>	<b>16</b>
<b>4.0 Reccomendations . . . . .</b>	<b>17</b>
<b>5.0 References . . . . .</b>	<b>18</b>

## List of Figures

Figure 1 — Nonlocal Neutron Density for ${}^4\text{He}$ with N <sup>4</sup> LO(500)+3N	5
Figure 2 — Nonlocal Nucleon Density for ${}^6\text{He}$ with NN+3N(400) .	6
Figure 3 — Local Nuclear Density for ${}^6\text{He}$ with NN+3N(400) . . .	7
Figure 4 — A-Nucleon Density Comparison . . . . .	7
Figure 5 — Local Nuclear Density for ${}^{16}\text{O}$ with N <sup>4</sup> LO(500)+3N . .	8
Figure 6 — Neutron $N_{\max}$ Convergence for ${}^6\text{He}$ with NN+3N(400)	9
Figure 7 — Log Proton $N_{\max}$ Convergence for ${}^6\text{He}$ with NN+3N(400) 10	10
Figure 8 — Nucleon Kinetic Density for ${}^{16}\text{O}$ with N <sup>4</sup> LO(500)+3N .	15
Figure 9 — Kinetic Density $N_{\max}$ Comparison for ${}^{16}\text{O}$ with N <sup>4</sup> LO(500)+3N 16	16

## 1.0 Introduction

There have been substantial advancements in developments of *ab initio* approaches to nuclear physics, from which it is possible to extract crucial quantities such as nuclear densities. Nonlocal translationally invariant nuclear density is a generalized form of the nuclear density constructed from shell model one body densities, consideration of quantum nonlocality, and the removal of the spurious center of mass (COM) component introduced by the choice of a single particle basis to describe the A-nucleon system.

The *ab initio* approach we use to solve the many-body Schrödinger equation for bound states is the no-core shell model (NCSM) [3], which begins with high precision two and three nucleon interactions. The NCSM employs the use of effective interactions calculated for large, but finite, expansions in the antisymmetrized A-nucleon harmonic oscillator (HO) many-body basis states. The basis truncation is determined by the parameter  $N_{\max}$ . A useful property of the HO basis is the preservation of translational invariance in the wavefunction when a single particle Slater Determinant (SD) basis is used with this truncation. For small nuclei, it is necessary to preserve this translational invariance.

In this report, two different high precision interactions were chosen to calculate the nuclear density. The first interaction is a two nucleon interaction at  $N^3LO$  with a 500 MeV cut-off developed by Entem and Machleidt, and a three nucleon interaction at  $N^2LO$  with a 400 MeV cut-off developed by Petr Navrátil. This is a standard interaction in nuclear physics, and will be denoted as NN+3N(400). The second interaction used is a two nucleon interaction at  $N^4LO$  with the two nucleon force systematic from

leading order to N<sup>4</sup>LO, developed in 2015 by Entem and Machleidt [2]. The three nucleon component of this interaction is at N<sup>2</sup>LO with simultaneous local and nonlocal regularization, developed by Petr Navrátil. The most important difference between these two interactions is that the second interaction developed in 2015 is a softer interaction. That is, the two nucleon component converges much faster than in the standard interaction, which provides nice properties for *ab initio* calculations.

The motivation for calculating the nonlocal translationally invariant nuclear density is the need for *ab initio* approaches to provide insight into nuclear structure, to act as input for construction of optical potentials, and to provide more accurate results for density functional theory. Often, approximations or “unphysical” densities are used in these areas, and so we are looking to benchmark the impact of nonlocal translationally invariant nuclear densities on these fields. Preliminary kinetic densities have been calculated for direct comparisons to density functional theorists and collaborations with colleagues at TRIUMF are underway for studying the optical potentials of <sup>16</sup>O.

## 2.0 Analysis

### 2.1 Nonlocal Translationally Invariant Nuclear Density

#### 2.1.1 Background

Two crucial issues are often not addressed correctly when calculating nuclear densities. Local densities are used as an approximation when, in general,

nonlocality of the density must be considered. The density operator can be generalized as outlined in Equation 1; the inclusion of a second coordinate such that the initial and final wavefunction states are acted upon by separate coordinates. For clarity,  $i$  denotes the particle number.

$$\rho_{op}(\vec{r}) = \sum_{i=1}^A \{|\vec{r}\rangle\langle\vec{r}|\}^i \longrightarrow \rho_{op}(\vec{r}, \vec{r}') = \sum_{i=1}^A \{|\vec{r}\rangle\langle\vec{r}'|\}^i \quad (1)$$

Another issue encountered is the contribution of a spurious centre of mass (COM) component to the nuclear density. This component comes from the chosen single particle basis (harmonic oscillator basis) and produces unphysical behaviour in the nuclear density. The choice of the HO basis is important as the factorization of the Jacobi and Slater Determinant eigenstates allows for the decoupling of the ground state COM component from the intrinsic part of the wavefunction, making the COM of the wavefunction removable. Note the groundstate COM component of the wavefunction  $\phi_{000}(\vec{\xi}_0)$  is separated from the intrinsic part of the wavefunction as illustrated in Equation 2.

$$\langle \vec{r}_1 \dots \vec{r}_A \vec{\sigma}_1 \dots \vec{\sigma}_A \vec{\tau}_1 \dots \vec{\tau}_A \rangle = \langle \vec{\xi}_1 \dots \vec{\xi}_{A-1} \dots \vec{\sigma}_A \vec{\tau}_1 \dots \vec{\tau}_A | A\lambda JM \rangle \phi_{000}(\vec{\xi}_0) \quad (2)$$

The local form of the nuclear density seen in Equation 3 containing the COM component is the most common form of nuclear density implemented in calculations. An important portion of the nuclear density are the one-body density matrix elements coming from second quantization, seen on the final line of Equation 3. Notable components of the nuclear density include the radial harmonic oscillator (RHO) and the spherical harmonics,  $R_{n,l}(r)$  and

$Y_K(\hat{r})$  respectively.

$$\begin{aligned}
{}_{SD}\langle A\lambda JM | \rho_{op}(\vec{r}) | A\lambda JM \rangle_{SD} = \\
\frac{1}{\hat{J}_f} \sum (J_i M_i K k | J_f M_f) Y_{Kk}^*(\hat{r}) R_{n_1, l_1}(r) R_{n_2, l_2}(r) \\
\times \langle l_1 \frac{1}{2} j_1 || Y_K || l_2 \frac{1}{2} j_2 \rangle \frac{-1}{\hat{K}} \\
\times {}_{SD}\langle A\lambda_f J_f || (a_{n_1, l_1, j_1}^\dagger \tilde{a}_{n_2, l_2, j_2})^{(K)} || A\lambda_i J_i \rangle
\end{aligned} \tag{3}$$

Beginning with the local, COM contaminated form of the nuclear density, one can derive a local translationally invariant nuclear density. This exact derivation was performed by P. Navrátil [4]. As mentioned previously, a local description of nuclear density is not general enough for nuclear theory. A nonlocal nuclear density which has the COM component removed is required, which has since been derived by P. Navrátil and implemented by our group. Extending the density from the local translationally invariant case to the nonlocal case is a trivial one, and so shown in Equation 4 is the nonlocal translationally invariant nuclear density.

$$\begin{aligned}
{}_{SD}\langle A\lambda_j J_j M_j | \rho_{op}(\vec{r} - \vec{R}, \vec{r}' - \vec{R}) | A\lambda_i J_i M_i \rangle_{SD} = \\
\left(\frac{A}{A-1}\right)^3 \sum \frac{1}{\hat{J}_f} (J_i M_i K k | J_f M_f) \left( \widehat{Y_l^*(\vec{r} - \vec{R})} \widehat{Y_{l'}^*(\vec{r}' - \vec{R})} \right)_k^{(K)} \\
\times R_{n,l} \left( \sqrt{\frac{A}{A-1}} |\vec{r} - \vec{R}| \right) R_{n',l'} \left( \sqrt{\frac{A}{A-1}} |\vec{r}' - \vec{R}| \right) \\
\times (M^K)_{n,l,n',l',n_1,l_1,n_2,l_2}^{-1} \frac{\sqrt{4\pi}(-1)^{l_1+l_2+k} \hat{K}}{\hat{l}_1 \hat{l}_2 (l_1 0 l_2 0 | K 0)} \langle l_1 \frac{1}{2} j_1 || Y_K || l_2 \frac{1}{2} j_2 \rangle \\
\times \frac{(-1)}{\hat{K}} {}_{SD}\langle A\lambda_f J_f || (a_{n_1, l_1, j_1}^\dagger \tilde{a}_{n_2, l_2, j_2})^{(K)} || A\lambda_i J_i \rangle
\end{aligned} \tag{4}$$

The density is normalized as follows, where A is the total number of nucleons.

$$\int d\vec{x} \langle A\lambda JM | \rho_{op}(\vec{x}) | A\lambda JM \rangle = A \tag{5}$$

### 2.1.2 Application to $^4\text{He}$ , $^6\text{He}$ , and $^{16}\text{O}$

In order to benchmark COM removal, calculations of the translationally invariant and COM contaminated nuclear density were performed for  $^4\text{He}$ ,  $^6\text{He}$ , and  $^{16}\text{O}$ . For the following plots, nuclear density which includes the COM will be referred to as “With COM” and those which are translationally invariant will be referred to as “TRINV”. Only the groundstate of the nuclei is considered and all angular dependence will be factorized out during plotting.

Consider the nonlocal neutron density of  $^4\text{He}$  seen in Figure 1. Comparing COM contaminated and TRINV plots shows a significant difference in the structure of the neutron density, which is identically true for the proton density. The most important feature changes in the nonlocal density include larger peak values and steeper slopes, in addition to a reduction in breadth.

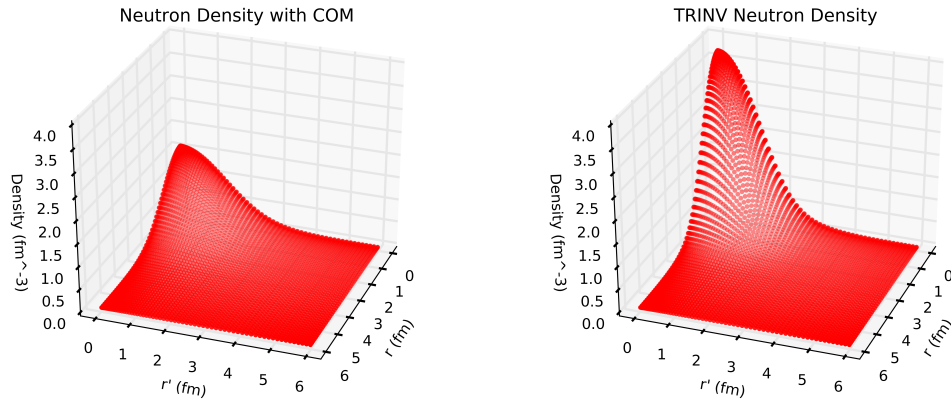


Figure 1: Nonlocal Neutron Density for  $^4\text{He}$  with  $\text{N}^4\text{LO}(500)+3\text{N}$

$^6\text{He}$  is a particularly interesting system to investigate due to the halo structure; the nucleus is composed of a central two proton and two neutron body being orbited by a neutron pair. Regarding the nonlocal nuclear density of  $^6\text{He}$  seen in Figure 2, we observe similar changes originally seen in

$^4\text{He}$ 's nuclear density. The TRINV nuclear density has a larger peak, steeper slopes, and a reduction in breadth. These changes to the structure of the density are consistent across the proton and neutron density, however the COM removal has a larger effect on the proton density features. Additionally, while the effects of COM removal are still quite large, there is a slightly smaller impact on the density structure changes of  $^6\text{He}$ .

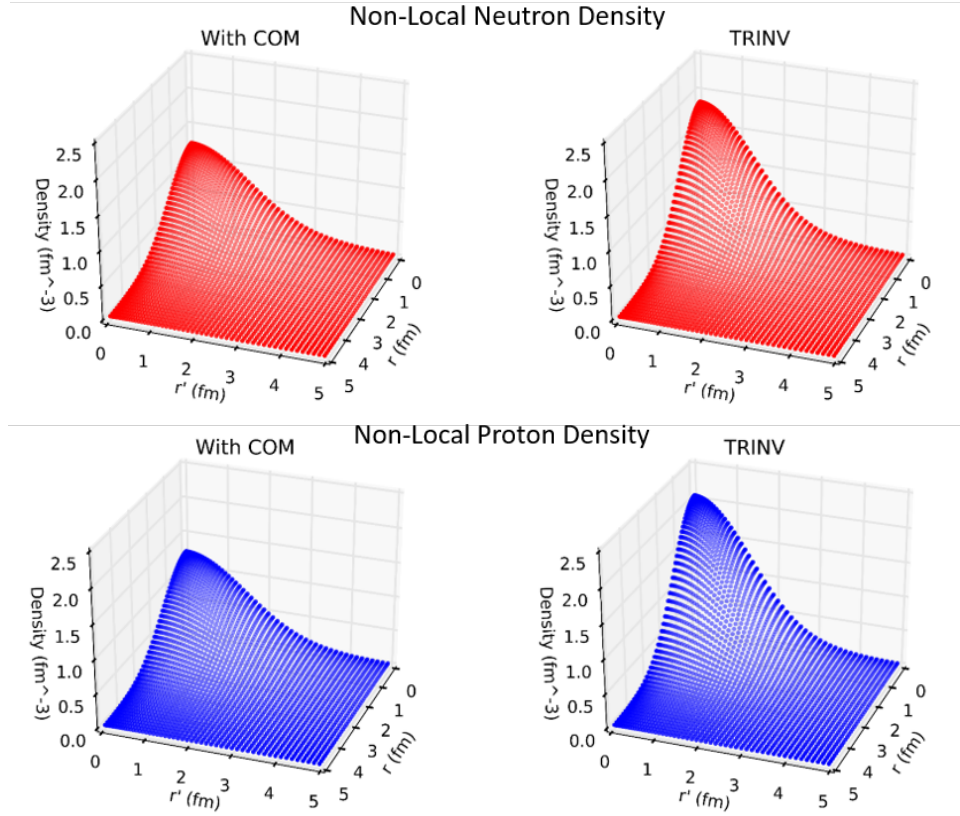


Figure 2: Nonlocal Nucleon Density for  $^6\text{He}$  with NN+3N(400)

The results of COM removal are better illustrated by considering the local nuclear density of  $^6\text{He}$  shown in Figure 3. Akin to the nonlocal density, significant changes in the peak of the nuclear density and an increase in the steepness of slope are observed. Here, the difference in effects on the proton and neutron densities is readily noticeable. Clearly, in  $^6\text{He}$ , COM removal

impacts the structure of the proton density more than the neutron density.

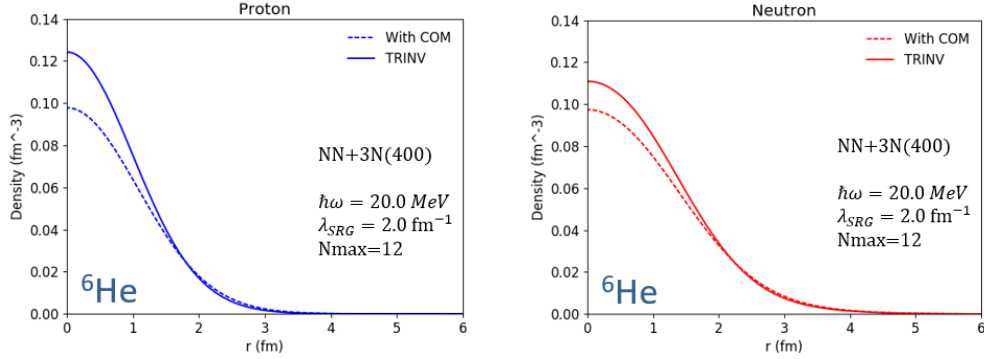


Figure 3: Local Nuclear Density for  ${}^6\text{He}$  with NN+3N(400)

Previous figures illustrate that the effects of COM removal are quite large in small nuclei, and as a result COM removal is seen to be a crucial step in calculating more physically accurate densities for optical potentials and results of high energy nuclear reactions. Consider Figure 4, where the effects of COM removal with increasing A-nucleon number are contrasted.

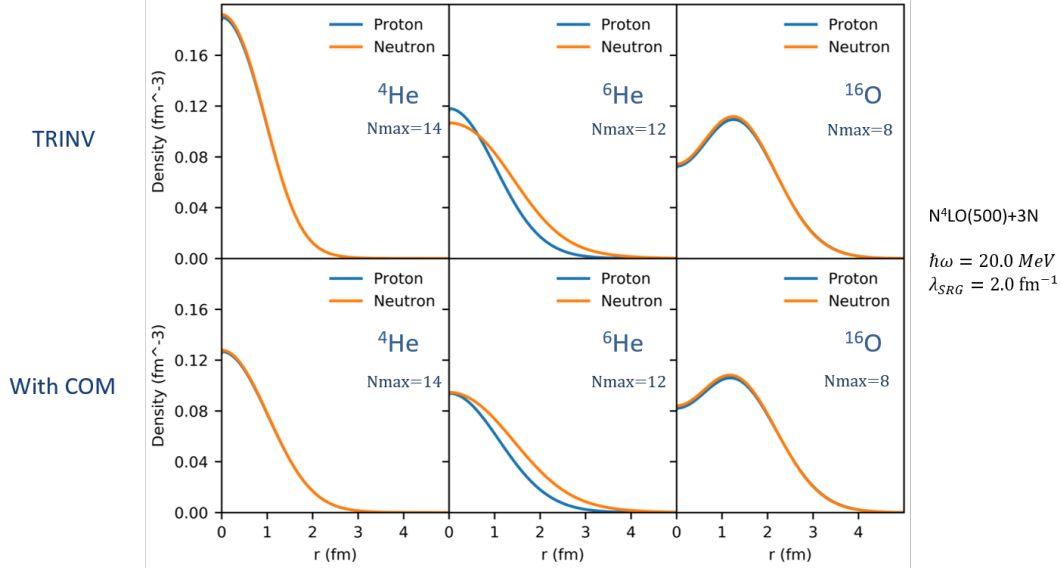


Figure 4: A-Nucleon Density Comparison

As shown by Figure 4, increasing A-nucleon number coincides with a reduction in the effects of COM removal. Notice the column of plots containing  $^{16}\text{O}$ . The differences of the COM contaminated density and the TRINV density are not nearly as drastic as the changes observed in  $^4\text{He}$  or  $^6\text{He}$ . This is to be expected as the COM component of the nuclear density scales as  $\frac{1}{A}$ . The larger the total nucleon number, the less prominent the COM component is in the wavefunction.

While this effect is reduced, studying the nucleon density of  $^{16}\text{O}$  reveals that COM removal is still has a non-negligible impact on the structure of the density. Notice the effects in Figure 5, especially at the short range.

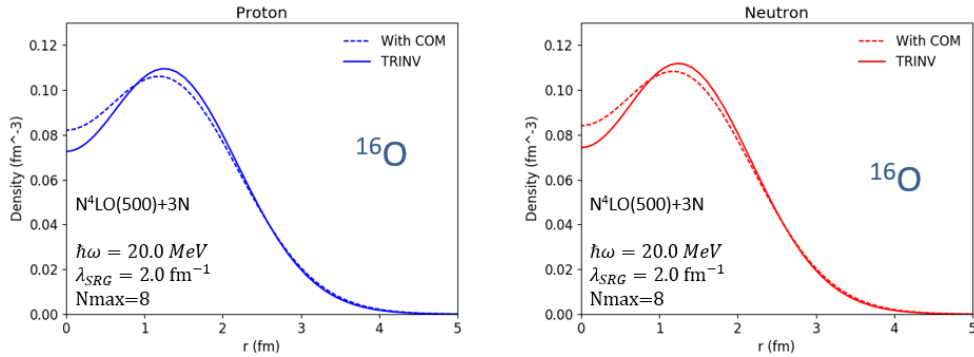


Figure 5: Local Nuclear Density for  $^{16}\text{O}$  with  $\text{N}^4\text{LO}(500)+3\text{N}$

In summary, COM removal is an important step in calculating more physically accurate nuclear densities. The density operator is now generalized to be nonlocal, allowing these nonlocal translationally invariant nuclear densities to be analytically included in optical potentials and high energy nuclear reactions. While the effect in larger nuclei is less significant, it is still important to benchmark the COM contaminated density with the translationally invariant density as applying different operators to the density may produce an amplification of effects from COM removal.

### 2.1.3 $N_{\max}$ Convergence

Given the complexity of the calculations, it is necessary to study the convergence of the neutron density in Figure 6. Each color corresponds to the neutron density with a different value of  $N_{\max}$ . The largest effect on convergence is observed at short range distances where we see the neutron density converge, with minimal difference from  $N_{\max}=10$  to  $N_{\max}=12$ . The convergence pattern is identical for the proton density.

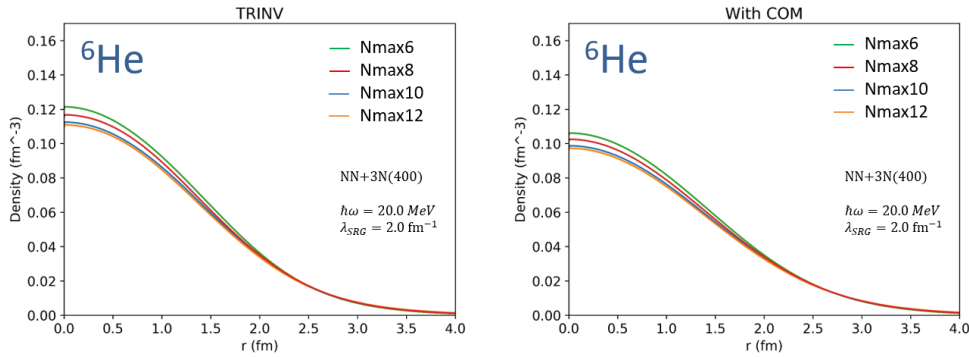


Figure 6: Neutron  $N_{\max}$  Convergence for  ${}^6\text{He}$  with NN+3N(400)

Essentially, these plots show that the nuclear densities being calculated converge with reasonable sizes of basis truncation. However, since the HO basis is used, the density displays unphysical asymptotic behaviour due to a Gaussian tail introduced by the basis expansion. Additionally, as we converge in the short range the wavefunction must compensate at long ranges in order satisfy the normalization condition displayed in Equation 5.

The long range behaviour described above can be seen in the logarithmic plot, Figure 7. The TRINV density approaches zero at a faster rate than the COM contaminated density. Note that while the density exhibits unphysical long range behaviour, the variations are on the order of  $10^{-9}$ .

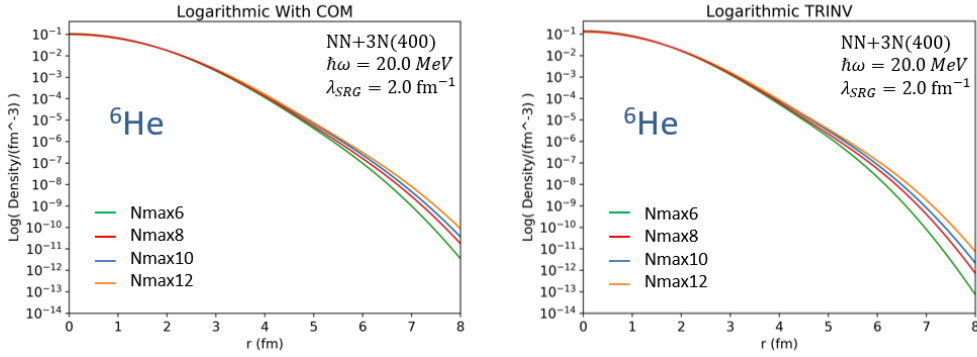


Figure 7: Log Proton  $N_{\max}$  Convergence for  ${}^6\text{He}$  with NN+3N(400)

## 2.2 Derivative of Radial Harmonic Oscillator

Several quantities which can be investigated with the nonlocal translationally invariant nuclear density depend on derivatives or gradients of the nonlocal density. Given that the nuclear density is proportional to the radial harmonic oscillator (RHO) function, any objects which are defined by derivative operations on the density will require an analytic representation for the derivative of the RHO. The derivation begins with considering the position basis representation of the RHO [1], which has parameter dependence on  $b$ , the oscillator length.

$$R_{n,l}(r) = \sqrt{\frac{2\Gamma(n+1)}{(b^2)^{l+3/2}\Gamma(n+l+3/2)}} r^l e^{\frac{-r^2}{b^2}} L_n^{l+1/2}\left(\frac{r^2}{b^2}\right) \quad (6)$$

Performing a derivative on the RHO generates three terms which can be written in terms of the RHO using the following relations.

$$\frac{d}{dx} L_n^k(x) = -L_{n-1}^{k+1}(x) \quad (7)$$

$$L_n^{k+1}(x) = L_n^k(x) + L_{n-1}^{k+1}(x) \quad (8)$$

$$c_{n,l,b} = \left( \frac{2\Gamma(n+1)}{(b^2)^{l+3/2}\Gamma(n+l+3/2)} \right)^{1/2} \quad (9)$$

Using Equation 7, the derivative can be written as follows.

$$\begin{aligned} \frac{d}{dr} R_{n,l}(r) &= c_{n,l,b} \left[ lr^{l-1} e^{\frac{-r^2}{b^2}} L_n^{l+1/2} \left( \frac{r^2}{b^2} \right) \right. \\ &\quad \left. - \frac{r^{l+1}}{b^2} e^{\frac{-r^2}{b^2}} L_n^{l+1/2} \left( \frac{r^2}{b^2} \right) + r^l e^{\frac{-r^2}{b^2}} \left( \frac{-2r}{b^2} L_{n-1}^{l+3/2} \left( \frac{r^2}{b^2} \right) \right) \right] \end{aligned} \quad (10)$$

$$\frac{d}{dr} R_{n,l}(r) = \frac{l}{r} R_{n,l}(r) - c_{n,l,b} \frac{r^{l+1}}{b^2} \left[ L_n^{l+1/2} \left( \frac{r^2}{b^2} \right) + 2L_{n-1}^{l+3/2} \left( \frac{r^2}{b^2} \right) \right] \quad (11)$$

Now applying Equation 8, it is possible to reduce the number of Laguerre polynomials in the expression. The Laguerre polynomials can then be written in terms of their respective RHO functions, resulting in the final expression for the derivative of the RHO shown in Equation 14.

$$\frac{d}{dr} R_{n,l}(r) = \frac{l}{r} R_{n,l}(r) - c_{n,l,b} \frac{r^{l+1}}{b^2} \left[ L_n^{l+3/2} \left( \frac{r^2}{b^2} \right) + L_{n-1}^{l+3/2} \left( \frac{r^2}{b^2} \right) \right] \quad (12)$$

$$\frac{d}{dr} R_{n,l}(r) = \frac{l}{r} R_{n,l}(r) - \frac{c_{n,l,b}}{b^2} \left[ \frac{R_n^{l+1}(r)}{c_{n,l+1,b}} + \frac{R_{n-1}^{l+1}(r)}{c_{n-1,l+1,b}} \right] \quad (13)$$

$$\frac{d}{dr} R_{n,l}(r) = \frac{l}{r} R_{n,l}(r) - \frac{1}{b} \left[ \sqrt{n+l+\frac{3}{2}} R_n^{l+1}(r) + \sqrt{n} R_{n-1}^{l+1}(r) \right] \quad (14)$$

## 2.3 Kinetic Density

The kinetic density of a nucleus is a direct application of the nuclear densities determined. Kinetic density is an essential object of density

functional theory, and is defined as

$$\tau(\vec{r}) = \vec{\nabla} \cdot \vec{\nabla}' \rho^{trinv}(\vec{r}, \vec{r}')|_{\vec{r}=\vec{r}'} \quad (15)$$

Kinetic density is investigated due to the dependence on gradients of the nuclear density. It is expected that the kinetic density would be more sensitive to changes in features of the nuclear density as a result of these gradients, and so the effect of COM removal we observed in nuclear densities should be amplified in the kinetic density results.

### 2.3.1 Derivation

In this derivation, only one component of the  $\vec{\nabla} \cdot \vec{\nabla}'$  product will be calculated due to the length of the derivation. The gradients are performed using spherical components of the nabla operator, and so the  $\nabla_0 \nabla_0'$  component will be derived. The same method is applied to the additional terms generated by  $\vec{\nabla} \cdot \vec{\nabla}'$ . The kinetic density can be written in the compressed form,

$$\begin{aligned} \tau_0 = \nabla_0 \nabla_0' & \left[ \sum_{n,l,n',l',K} \beta_{n,l,n',l',K}^{IS,FS} \left( Y_l^*(\widehat{\vec{r} - \vec{R}}) Y_{l'}^*(\widehat{\vec{r}' - \vec{R}}) \right)_k^{(K)} \right. \\ & \left. R_{n,l} \left( \sqrt{\frac{A}{A-1}} |\vec{r} - \vec{R}| \right) R_{n',l'} \left( \sqrt{\frac{A}{A-1}} |\vec{r}' - \vec{R}| \right) \right] \end{aligned} \quad (16)$$

For legibility, the arguments of the radial harmonic oscillator functions and spherical harmonics will be omitted. Instead, refer to the primed quantum number to dictate which coordinate each object contains in the argument.

$$\tau_0 = \nabla_0' \left[ \sum_{n,l,n',l',K} \beta_{n,l,n',l',K}^{IS,FS} R_{n,l} R_{n',l'} \left( Y_l^* Y_{l'}^* \right)_k^{(K)} \right] \quad (17)$$

Uncoupling the spherical harmonics, both nabla operators can be applied to their respective coordinates.

$$\tau_0 = \sum_{n,l,n',l',K,m_l,m_{l'}} (lm_l l' m_{l'} | K k) \beta_{n,l,n',l',K}^{IS,FS} \left[ \nabla_0 R_{n,l} Y_l^* \right] \left[ \nabla_0' R_{n',l'} Y_{l'}^* \right] \quad (18)$$

Using properties of the nabla operator in spherical coordinates, we see that

$$\begin{aligned} \nabla_0 R_{n,l} Y_l^* &= \sqrt{\frac{(l+1)^2 - m_l^2}{(2l+1)(2l+3)}} \left( \frac{dR_{n,l}}{dr} - \frac{l}{r} R_{n,l} \right) Y_{l+1,m_l}^* \\ &\quad - \sqrt{\frac{l^2 - m_l^2}{(2l-1)(2l+1)}} \left( \frac{dR_{n,l}}{dr} + \frac{l+1}{r} R_{n,l} \right) Y_{l-1,m_l}^* \end{aligned} \quad (19)$$

This relation is general. Expanding the  $\nabla_0 R_{n,l} Y_l^*$  and  $\nabla_0' R_{n',l'} Y_{l'}^*$  product creates four terms with complicated coefficients. Four “ $c_{ij}$ ” coefficients are introduced to reduce the amount of angular momentum algebra shown.

$$\begin{aligned} c_{00} &= \sqrt{\frac{(l+1)^2 - m_l^2}{(2l+1)(2l+3)}} \left( \frac{dR_{n,l}}{dr} - \frac{l}{r} R_{n,l} \right) \\ &\quad \times \sqrt{\frac{(l'+1)^2 - m_{l'}^2}{(2l'+1)(2l'+3)}} \left( \frac{dR_{n',l'}}{dr'} - \frac{l'}{r'} R_{n',l'} \right) \end{aligned} \quad (20)$$

$$\begin{aligned} c_{01} &= \sqrt{\frac{(l+1)^2 - m_l^2}{(2l+1)(2l+3)}} \left( \frac{dR_{n,l}}{dr} - \frac{l}{r} R_{n,l} \right) \\ &\quad \times \sqrt{\frac{l'^2 - m_{l'}^2}{(2l'-1)(2l'+1)}} \left( \frac{dR_{n',l'}}{dr'} + \frac{l'+1}{r'} R_{n',l'} \right) \end{aligned} \quad (21)$$

$$\begin{aligned} c_{02} &= \sqrt{\frac{l^2 - m_l^2}{(2l-1)(2l+1)}} \left( \frac{dR_{n,l}}{dr} + \frac{l+1}{r} R_{n,l} \right) \\ &\quad \times \sqrt{\frac{(l'+1)^2 - m_{l'}^2}{(2l'+1)(2l'+3)}} \left( \frac{dR_{n',l'}}{dr'} - \frac{l'}{r'} R_{n',l'} \right) \end{aligned} \quad (22)$$

$$c_{03} = \sqrt{\frac{l^2 - m_l^2}{(2l-1)(2l+1)}} \left( \frac{dR_{n,l}}{dr} + \frac{l+1}{r} R_{n,l} \right) \\ \times \sqrt{\frac{l'^2 - m_{l'}^2}{(2l'-1)(2l'+1)}} \left( \frac{dR_{n',l'}}{dr'} + \frac{l'+1}{r'} R_{n',l'} \right) \quad (23)$$

With these coefficients defined, the expansion becomes

$$\left[ \nabla_0 R_{n,l} Y_l^* \right] \left[ \nabla_0' R_{n',l'} Y_{l'}^* \right] = c_{00} Y_{l+1,m_l}^* Y_{l'+1,m_{l'}}^* + c_{01} Y_{l+1,m_l}^* Y_{l'-1,m_{l'}}^* \quad (24)$$

$$c_{02} Y_{l-1,m_l}^* Y_{l'+1,m_{l'}}^* + c_{03} Y_{l-1,m_l}^* Y_{l'-1,m_{l'}}^*$$

Evaluating these terms at  $\vec{r} = \vec{r}'$ , we can recouple each pair of spherical harmonics into a single spherical harmonic by coupling the  $l$  and  $l'$  angular momenta, producing an angular momentum factor and two clebsch-gordan coefficients. Four “ $d_{ij}$ ” coefficients are introduced to further reduce the amount of angular momentum algebra shown.

$$d_{00} = \sqrt{\frac{(2l+3)(2l'+3)}{4\pi(2L+1)}} (l+1\ m_l\ l'+1\ m_{l'}|LM)(l+1\ 0\ l'+1\ 0|LM) \quad (25)$$

$$d_{01} = \sqrt{\frac{(2l+3)(2l'-1)}{4\pi(2L+1)}} (l+1\ m_l\ l'-1\ m_{l'}|LM)(l+1\ 0\ l'-1\ 0|LM) \quad (26)$$

$$d_{02} = \sqrt{\frac{(2l-1)(2l'+3)}{4\pi(2L+1)}} (l-1\ m_l\ l'+1\ m_{l'}|LM)(l-1\ 0\ l'+1\ 0|LM) \quad (27)$$

$$d_{04} = \sqrt{\frac{(2l-1)(2l'-1)}{4\pi(2L+1)}} (l-1\ m_l\ l'-1\ m_{l'}|LM)(l-1\ 0\ l'-1\ 0|LM) \quad (28)$$

With these coefficients defined, it becomes possible to sum over a collective index for L and factorize out the spherical harmonics. This reduces the

expression for  $\tau_0$  to

$$\begin{aligned} \tau_0 = & \sum_{n,l,n',l',K,m_l,m_{l'}} (lm_l l' m_{l'} | Kk) \beta_{n,l,n',l',K}^{IS,FS} Y_{LM}^* \\ & \times \left[ c_{00}|_{\vec{r}=\vec{r}'} d_{00} + c_{01}|_{\vec{r}=\vec{r}'} d_{01} + c_{02}|_{\vec{r}=\vec{r}'} d_{02} + c_{03}|_{\vec{r}=\vec{r}'} d_{03} \right] \end{aligned} \quad (29)$$

as required.

### 2.3.2 Kinetic Density of $^{16}\text{O}$

Shown in Figure 8 are **preliminary** results for the kinetic density of  $^{16}\text{O}$ . The plots show an enormous difference between the COM contaminated and the translationally invariant kinetic density. We are skeptical that the results are correct given that we do not see convergence in the COM contaminated kinetic density, which will be discussed later. If however, the results are correct, this will have very severe implications for density functional theory, as the structure observed is incredibly different from the structure which would normally be used.

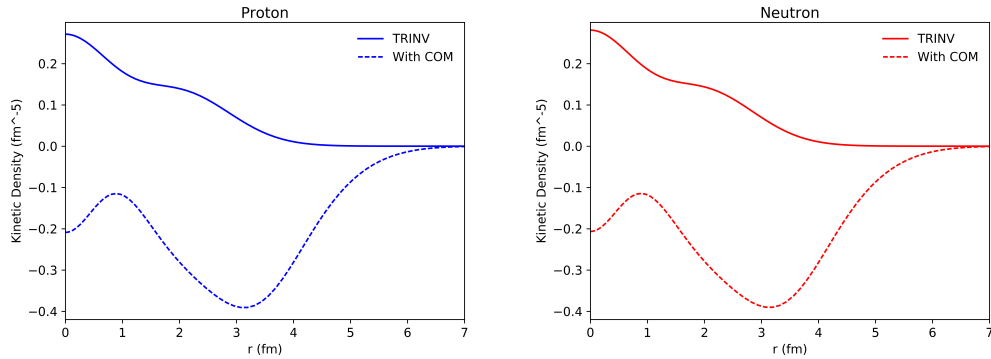


Figure 8: Nucleon Kinetic Density for  $^{16}\text{O}$  with  $\text{N}^4\text{LO}(500)+3\text{N}$

The TRINV is noticeably smoother and always positive, whereas the COM

contaminated density is always negative and contains several fluctuations. Methods by which the kinetic density can be benchmarked are being explored, including determining a relationship between the integral of kinetic density and the kinetic energy of the wavefunction.

As a brief look at convergence, consider Figure 9. Each color corresponds to the proton kinetic density of  $^{16}\text{O}$  with a different  $N_{\max}$  value. The TRINV density does show convergence for the kinetic density within reasonable basis expansions.

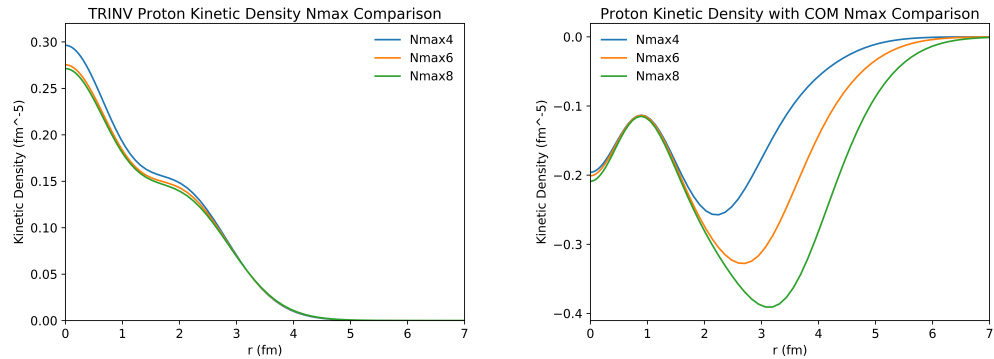


Figure 9: Kinetic Density  $N_{\max}$  Comparison for  $^{16}\text{O}$  with  $\text{N}^4\text{LO}(500)+3\text{N}$

However, studying the COM contaminated plot reveals no such convergence, leading us to believe that either the unphysical density will not converge in our current model spaces, or the implementation is incorrect. The latter is currently being investigated at TRIUMF.

### 3.0 Conclusions

In conclusion, significant differences in the density of light nuclei were observed when the process of COM removal was performed. This leads us to

decide that for nuclear reactions involving small nuclei, COM removal is an essential step in ensuring the most physically accurate density is calculated.

Additionally, we can now use the more general, nonlocal nuclear density for constructing optical potentials of nuclei and within density functional theory.

## 4.0 Reccomendations

It is recommended that all calculations using light nuclei now use the local/nonlocal translationally invariant nuclear density when performing theoretical predictions for high energy nuclear reactions.

In addition, it is recommended that the kinetic density be further benchmarked in order to ensure it is correct, which can be done in several ways. Initially, direct checks with density functional theorists would allow us to benchmark whether or not the COM contaminated is correct. Additional checks which could be performed to benchmark the translationally invariant kinetic density include finding a relation between the kinetic energy of the wavefunction and the integral of the kinetic density. As the kinetic energy of the wavefunction is very well known, being able to compare these values would provide excellent benchmarking for calculations of kinetic density.

## 5.0 References

1. Bohr, A. (2008). Nuclear structure. New Jersey: World Scientific.
2. D. R. Entem, N. Kaiser, R. Machleidt, and Y. Nosyk, Phys. Rev. C 91, 014002 (2015).
3. P. Navrátil, J. P. Vary, and B. R. Barrett, Phys. Rev. Lett. **84**, 5728 (2000); Phys. Rev. C **62**, 054311 (2000).
4. P. Navrátil, Phys. Rev. C **70**, 014317 (2004).